ELSEVIER

Journal of Non-Crystalline Solids 188 (1995) 136–146

JOURNAL OF NON-CRYSTALLINE SOLIDS

Glass formation and crystallization in Li_2O–Na_2O–K_2O–SiO_2

R. Ota *, T. Wakasugi, W. Kawamura, B. Tuchiya, J. Fukunaga

Department of Chemistry and Materials Technology, Kyoto Institute of Technology, Matsugasaki, Sakyo-ku, Kyoto 606, Japan

Received 25 March 1994; revised manuscript received 4 January 1995

Abstract

Glass-forming regions in the Li_2O–Na_2O-$mSiO_2$ ($m = 2$ or 1.5) and Li_2O–Na_2O–K_2O–$mSiO_2$ ($m = 2$ or 1.5) systems were determined with various cooling rates. Viscosity and liquidus temperature were measured. Eutectics were observed in these systems. The critical cooling rate shows a minimum and the liquidus viscosity shows a maximum. It was found that Li_2O–Na_2O–$mSiO_2$ showed more extensive glass-forming ability than Li_2O–$mSiO_2$, Na_2O–$mSiO_2$ or K_2O–$mSiO_2$. Li_2O–Na_2O–K_2O–$mSiO_2$ shows an even larger glass-forming ability than Li_2O–Na_2O–$mSiO_2$. The significant role of mixing entropy or liquidus viscosity in the glass-forming kinetics of mixed alkali silicate systems is recognized.

1. Introduction

The glass-forming tendency of a melt is related to the viscosity at the liquidus (liquidus viscosity). Ota and Kunugi proposed a glass-forming criterion of a multi-component system in terms of the liquidus viscosity [1] and showed qualitative agreement between the compositional dependence of the critical cooling rates and liquidus viscosities for Li_2O–B_2O_3 [2], Na_2O–B_2O_3 [3–6], Li_2O–SiO_2 [7], Na_2O–GeO_2 [8], $NaPO_3$–$MnCl_2$ [9], $ZnCl_2$–$PbCl_2$–KCl [10] and Bi_2O_3–CuO–BaO [11]. Havermans et al. [12] reported the critical cooling rate for Na_2O–K_2O–SiO_2 and single alkali systems, Li_2O–SiO_2, Na_2O–SiO_2 and K_2O–SiO_2. They showed that mixed alkali systems exhibit a lower critical cooling rate than either of the single alkali systems. Mazurin [13] interpreted the compositional dependency of the critical cooling rate of the M_2O–SiO_2 system (M = Li, Na and K) by Havermans et al. [12] in term of the liquidus viscosity after the proposition of Ota and Kunigi [1]. Theoretically, the critical cooling rate, Q^*, is a function of the liquidus viscosity, η_L, the activation energy for viscous flow, E, and the fusion entropy ΔS_f [6,14] etc. (See Eq. (9) of the Appendix). It is obvious from Eq. (7) in the Appendix that Q^* decreases, i.e., glass formation is favored, with increasing η_L, E/T_L, ΔS_f, flow unit, V, and Fulcher's constant, T_0/T_L, and with decreasing T_L. It is expected that the eutectic composition is favored for glass formation because, even if the isothermal viscosity, η_T, and E change monotonically with composition, η_L and E/T_L terms will rise at the eutectic composition where T_L falls to a minimum. ΔS_f may assume a maximum at the eutectic composition. It seems that the viscosity-related terms (η_L and E/T_L) and the entropy-related terms play a decisive role in the glass-forming kinetics. In mixed alkali systems the mixing entropy of the alkali ions will contribute to increase the fusion entropy. The increase of ΔS_f,

* Corresponding author. Tel: +81-75 724 7565. Telefax: +81-75 724 7580. E-mail: waka@ipc.kit.ac.jp.

SSDI 0022-3093(95)00185-9

consequently, will lower the liquidus temperature. Thus enhanced glass formation is foreseen in the mixed alkali systems. In the present study, the glass-forming tendency of mixed alkali silicate, $(1-x)Li_2O$–$(x)Na_2O$–$mSiO_2$ ($m = 2$ or 1.5) and $(1-y)(0.4Li_2O \cdot 0.6Na_2O)$–$(y)K_2O$–$mSiO_2$ ($m = 2$ or 1.5) was studied.

2. Experimental

Glass samples for critical cooling rate determination were prepared by melt quenching using reagent-grade alkali carbonate (M_2CO_3; M = Li, Na and K) and quartz powder (SiO_2). The composition was $x = 0$–1.0 in the series $(1-x)Li_2O$–$(x)Na_2O$–$mSiO_2$ ($m = 2$ or 1.5) and $y = 0$–1.0 in the series $(1-y)(0.4Li_2O \cdot 0.6Na_2O)$–$(y)K_2O$–$mSiO_2$ ($m = 2$ or 1.5). The $0.4Li_2O \cdot 0.6Na_2O \cdot 2SiO_2$ composition is a eutectic composition of the Li_2O–Na_2O–$2SiO_2$ system (see Fig. 3(a) below). Batches were melted in a platinum crucible at 1300–1550°C for 30–60 min, and the molten glass was cast onto an iron plate. 10 g of glass in a Pt crucible was cooled to below T_g at various cooling rates, Q_1–Q_{11}, listed in Table 1. Q is the mean cooling rate between the liquidus temperature and T_g. Q ranged from 1.6×10^{-4} K/s (Q_1) by programmed furnace cooling to 59 K/s (Q_{11}) by plate press cooling. Table 1 shows that 69 days are required to cool the 1000°C temperature gap with Q_1 and only 17 s with Q_{11}.

Table 1
Cooling methods and mean-cooling rates, Q_1–Q_{11}, employed to determine the critical cooling rate for glass formation; 10 g melt in a platinum crucible of 20 cm^3 capacity was used for each cooling

	Method	Cooling rate, $\log(Q/K\,s^{-1})$	Time to cool (1000°C)
Q_1	Programmed cool	−3.78	69 days
Q_2	Programmed cool	−3.48	35 days
Q_3	Programmed cool	−3.08	14 days
Q_4	Programmed cool	−2.60	5 days
Q_5	Programmed cool	−2.38	3 days
Q_6	Programmed cool	−2.00	1 day
Q_7	Programmed cool	−1.48	8 h
Q_8	Furnace cool	−1.09	3 h
Q_9	Crucible air cool	0.11	13 min
Q_{10}	Air cool on iron plate	1.20	1 min
Q_{11}	Crucible water cool	1.77	17 s

Possible devitrification was inspected on the surface as well as in the interior of the quenched specimen with optical microscopy. The devitrified phases were identified by X-ray diffraction (XRD) with a polarizing microscope.

T_L was determined by the quenching method, whereby 100 mg of powdered glass sample, wrapped in a platinum foil was kept in an oven at various temperatures for at least 100–200 h. After being dropped into a carbon tetrachloride bath, the solidified specimen was checked for devitrification by optical microscopy.

The viscosity of the molten glass was measured in the temperature range of 370–1400°C. Three types of viscometer were employed according to the viscosity range: a counter balancing viscometer in the range $\eta = 0.1$–10^3 Pa s; a penetration viscometer [15] in the range $\eta = 10^3$–10^5 Pa s; and a beam-bending viscometer [15] in the range $\eta = 10^5$–10^{12} Pa s.

T_g was determined from dilatometry with a heating rate of 3 K/min. T_g is regarded as the temperature at which the viscosity, reaches 10^{12} Pa s.

3. Results

The variation of glass-forming regions with cooling rates, Q_1–Q_{11}, is illustrated in Fig. 1(a) for the Li_2O–Na_2O–SiO_2 system, and Fig. 1(b) for the $0.4Li_2O \cdot 0.6Na_2O$–K_2O–$2SiO_2$ system. The solid line indicates the critical cooling rate, Q^*, for glass formation. Results are summarized in Table 2(a)–(d).

In the $(1-x)Li_2O$–$(x)Na_2O$–$2SiO_2$ series (Fig. 1(a)), Q^* decreases from 1 K/s at the composition $x = 0$ to a minimum 5×10^{-4} K/s at the composition $x = 0.8$–0.9, and then increases to 1.7×10^{-3} K/s at the composition $x = 1.0$. In the $(1-y)(0.4Li_2O \cdot 0.6Na_2O)$–$(y)K_2O$–$2SiO_2$ series (Fig. 1(b)), most of the compositions do not show crystallization with the slowest cooling rate, Q_1, except at the compositions $y = 0$ and 0.9–1.0. Q^* is 1.2×10^{-3} K/s in the $y = 0$–0.1 range, and increases from 3.2×10^{-4} K/s at the composition $y = 0.9$ to 1.6×10^{-3} K/s at the composition $y = 1.0$. Figs. 2(a) and (b) indicate the glass-forming regions and

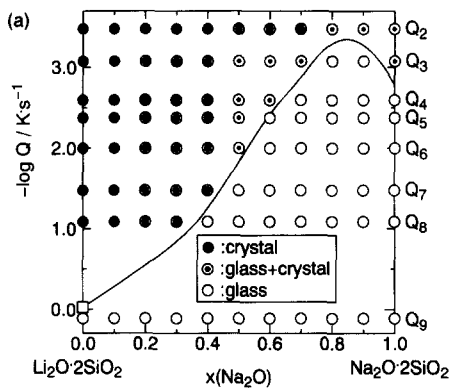

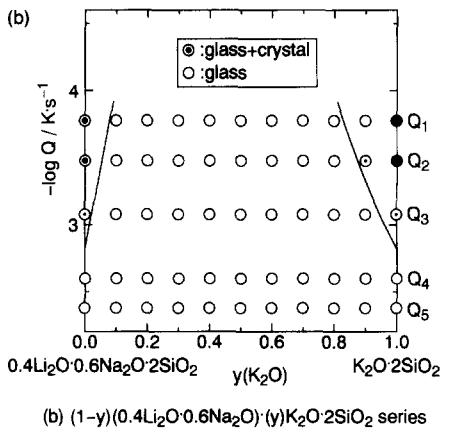

Fig. 1. Glass-forming regions at various cooling rates and critical cooling rate (solid line) in the $(1-x)Li_2O$–$(x)Na_2O$–$2SiO_2$ series (a) and $(1-y)$ $(0.4Li_2O \cdot 0.6Na_2O)$–$(y)K_2O$–$2SiO_2$ series (b). Open circles (○) are glass, closed circles (●) crystal, and double circles (◎) partially crystallized glass. Inner portion indicates the crystallized portion. Square (□) indicates data by Ota et al. [7] for the critical cooling rate in the $Li_2O \cdot 2SiO_2$ composition.

critical cooling rate for the Li_2O–Na_2O–$1.5SiO_2$ and $0.4Li_2O \cdot 0.6Na_2O$–K_2O–$1.5SiO_2$ systems. Fig. 2(a) indicates that Q^* decreases from 4.6×10^1 K/s at $x = 0$ to a minimum of 1×10^{-2} K/s at the composition $x = 0.8$–0.9, and then increases to 5.2×10^{-2} K/s at $x = 1.0$. In Fig. 2(b) Q^* is 5.2×10^{-2} K/s at $y = 0$ and is 5.1×10^{-2} K/s at $y = 1.0$ Q^* becomes less than 10^{-4} K/s at the composition $y = 0.4$–0.6.

The variation of liquidus temperature, T_L, in the Li_2O–Na_2O–K_2O–$mSiO_2$ system, ($m = 2$ or 1.5), is listed in Table 2(a)–(d) and shown in Figs. 3 and 4. The maximum error in the measurements is ±5°C. Fig. 3(a) indicates that T_L decreases from 1040°C at the composition $x = 0$ to an apparent eutectic 755°C at the composition $x = 0.6$, and then increases to 860°C at $x = 1.0$. The phase diagrams of the $Li_2O \cdot 2SiO_2$–$Na_2O \cdot 2SiO_2$ system by Kracek [16] and West [17] show eutectics at $x = 0.7$ and $x = 0.65$,

Table 2
Critical cooling rate, Q^*(K s^{-1}), liquidus temperature, T_L(°C), glass transition temperature, T_g(°C) and liquidus viscosity, η_L(Pas) of the $(1-x)Li_2O$–$(x)Na_2O$–$2SiO_2$ series (a), $(1-y)(0.4Li_2O \cdot 0.6Na_2O)$–$(y)K_2O$–$2SiO_2$ series (b), $(1-x)Li_2O$–$(x)Na_2O$–$1.5SiO_2$ series (c) and $(1-y)(0.4Li_2O \cdot 0.6Na_2O)$–$(y)K_2O$–$1.5SiO_2$ series (d)

x, y	$-\log(Q^*$ / K $s^{-1})$	T_L (°C)	T_g (°C)	log (η_L /Pa s)
(a) $(1-x)Li_2O$–$(x)Na_2O$–$2SiO_2$ series				
0.0	0.00	1043	437	1.34
0.1	0.86	1013	413	1.37
0.2	1.00	985	405	1.48
0.3	1.24	937	390	1.63
0.4	2.09	885	387	1.89
0.5	2.50	822	383	2.21
0.6	2.91	744	383	3.05
0.7	3.30	778	382	3.02
0.8	3.28	808	384	2.73
0.9	2.94	836	401	2.77
1.0	2.76	862	435	2.83
(b) $(1-y)(0.4LiO \cdot 0.6Na_2O)$–$(y)K_2O$–$2SiO_2$ series				
0.0	2.91	744	383	3.05
0.1	–	718	375	3.35
0.2	–	674	380	4.03
0.3	–	648	380	4.38
0.4	–	643	380	4.53
0.5	–	650	385	4.56
0.6	–	732	384	3.87
0.7	–	825	398	3.27
0.8	–	881	386	2.99
0.9	3.47	935	430	2.78
1.0	2.89	1036 [a]	484	2.31
(c) $(1-x)Li_2O$–$(x)Na_2O$–$1.5SiO_2$ series				
0.0	−1.66	926	400	0.48
0.1	−1.52	861	373	0.60
0.2	−1.30	804	353	0.77
0.3	−0.97	725	354	0.86
0.4	−0.47	806	355	1.15
0.5	0.23	899	367	1.60
0.6	1.28	965	360	2.23
0.7	2.00	1022	374	3.11
0.8	2.00	1074	378	2.55
0.9	2.03	1112	393	2.28
1.0	1.28	1144	421	2.07

Table 2 (continued)

x, y	$-\log(Q^*/K\,s^{-1})$	T_L (°C)	T_g (°C)	log (η_L /Pa s)
(d) $(1-y)(0.4Li_2O\cdot 0.6Na_2O)$–$(y)K_2O$–$1.5SiO_2$				
0.0	1.28	806	355	2.23
0.1	1.86	772	332	2.47
0.2	2.52	742	325	2.76
0.3	3.40	704	323	3.25
0.4	–	639	322	3.99
0.5	–	705	342	3.35
0.6	–	803	342	2.69
0.7	3.42	866	351	2.43
0.8	3.14	913	375	2.20
0.9	2.15	955	399	2.22
1.0	1.29	996	460	2.25

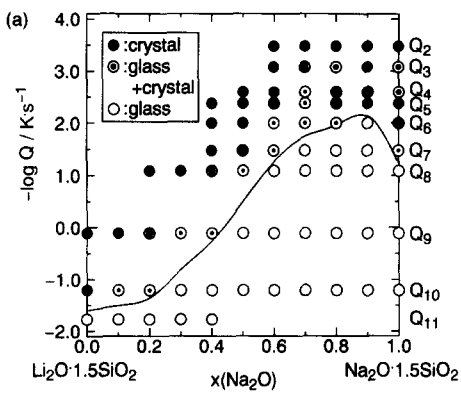

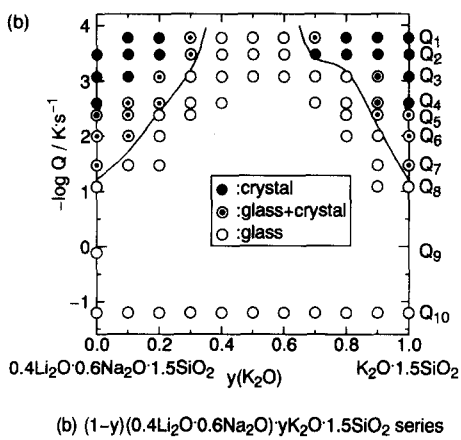

Fig. 2. Glass-forming regions and critical cooling rate (solid line) in the $(1-x)Li_2O$–$(x)Na_2O$–$1.5SiO_2$ series (a) and $(1-y)(0.4Li_2O$–$0.6Na_2O)$–$(y)K_2O$–$1.5SiO_2$ series (b). Open circles (○) denote glass, closed circles (●) crystal, and double circles (⊙) partially crystallized glass. Inner portion of the double circles indicates the crystallized portion.

respectively. Fig. 3(b) shows that there is a quasi-eutectic 650°C at the composition $y = 0.4$–0.5. Fig. 4(a) shows that T_L decreases from 1140°C at the composition $x = 0$ to eutectic of 700°C at the composition $x = 0.7$, and then increases to 920°C at the composition $x = 1.0$. Fig. 4(b) shows that T_L decreases from 800°C at $y = 0$ to a quasi-eutectic 620°C at the composition $y = 0.4$–0.5, and increases to 700°C at the composition $y = 1.0$.

Viscosity isotherms of the Li_2O–Na_2O–K_2O–$mSiO_2$ ($m = 2$ or 1.5) systems are summarized in a temperature range of 370–1300°C in Table 3(a)–(b)

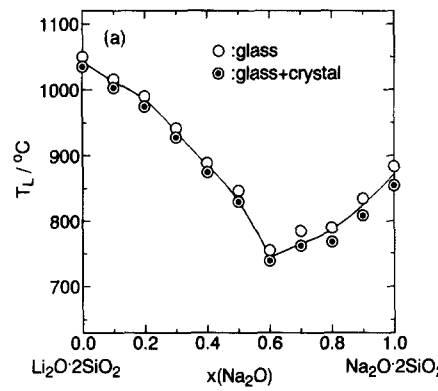

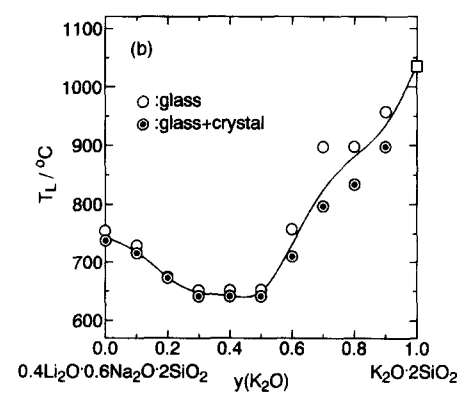

Fig. 3. Liquidus temperatures (solid line) of the $(1-x)Li_2O$–$(x)Na_2O$–$2SiO_2$ series (a) and $(1-y)(0.4Li_2O\cdot 0.6Na_2O)$–$(y)K_2O$–$2SiO_2$ series (b). Open circles (○) denote glass and double circles (⊙) partially crystallized glass. Square (□) indicates the data of Kracek [16].

Table 3
Viscosity isotherms of the Li_2O–Na_2O–K_2O–$mSiO_2$ glass ($m = 2$ or 1.5)

(a) $(1-x)Li_2O$–$(x)Na_2O$–$2SiO_2$ series [$\log(\eta_L/\text{Pa s})$]

x:	0.0	0.1	0.2	0.3	0.4	0.5	0.6	0.7	0.8	0.9	1.0
T(°C)											
380	–	–	–	–	–	–	11.81	–	–	–	–
400	–	–	–	11.89	11.67	11.53	11.32	11.38	11.60	12.05	–
420	–	11.94	11.68	11.46	10.54	10.46	10.13	10.33	10.64	11.64	–
440	11.91	11.26	10.64	10.35	9.36	9.24	9.10 [a]	9.26 [a]	9.42	10.58	11.78
460	11.35	10.26	9.57	9.40 [a]	8.49 [a]	8.43 [a]	8.40 [a]	8.51 [a]	8.68 [a]	9.32	11.35
480	10.38	9.34 [a]	8.79 [a]	8.73 [a]	7.73 [a]	7.74 [a]	7.78 [a]	7.85 [a]	8.00 [a]	8.62 [a]	10.27
500	9.35 [a]	8.66 [a]	8.11 [a]	8.11 [a]	7.07 [a]	7.06	7.03	7.46	7.20	8.00 [a]	9.46 [a]
550	7.75 [a]	7.21 [a]	6.70 [a]	6.79 [a]	5.76 [a]	5.56	5.80	6.14	5.88	6.70 [a]	8.08 [a]
600	6.50 [a]	6.05 [a]	5.59 [a]	5.71 [a]	4.78 [a]	4.86 [a]	4.84	5.10 [a]	5.22 [a]	5.68 [a]	6.94 [a]
700	4.64 [a]	4.32 [a]	3.98 [a]	4.04 [a]	3.41 [a]	3.42 [a]	3.56	3.73 [a]	3.83 [a]	4.18 [a]	5.17 [a]
800	3.33 [a]	3.08 [a]	2.85 [a]	2.81 [a]	2.49 [a]	2.42 [a]	2.69 [a]	2.78 [a]	2.86 [a]	3.12 [a]	3.86 [a]
900	2.36 [a]	2.15 [a]	2.02 [a]	1.88	1.84	1.77	1.94	2.08 [a]	2.15 [a]	2.35 [a]	2.86 [a]
1000	1.61 [a]	1.45	1.39	1.39	1.37	1.35	1.48	1.54	1.61	1.78	2.06
1100	1.11	1.01	0.98	0.95	0.98	0.99	1.08	1.13	1.21	1.33	1.60
1200	0.76	0.65	0.65	0.61	0.66	0.69	0.73	0.78	0.84	0.95	1.20
1300	0.47	0.37	0.38	0.30	0.39	0.43	0.44	0.45	0.55	0.65	0.85

(b) $(1-y)(0.4Li_2O \cdot 0.6Na_2O)$–$(y)K_2O$–$2SiO_2$ series [$\log(\eta_L/\text{Pa s})$]

y:	0.0	0.1	0.2	0.3	0.4	0.5	0.6	0.7	0.8	0.9	1.0
T(°C)											
370	–	–	12.02	11.98	11.96	–	–	–	–	–	–
380	11.81	11.83	11.82	11.75	11.81	12.04	–	–	–	–	–
400	11.32	11.02	10.80	10.92	11.02	11.47	11.79	12.06	12.00	–	–
420	10.13	9.94	9.95	9.87	9.97	10.52	11.01	11.56	11.64	–	–
440	9.10 [a]	8.82 [a]	8.89 [a]	8.74 [a]	8.83 [a]	9.48	10.04	10.62	11.17	11.84	–
460	8.40 [a]	8.09 [a]	8.22 [a]	8.07 [a]	8.17 [a]	8.80 [a]	9.20 [a]	9.66	10.20	11.37	12.04
480	7.78 [a]	7.44 [a]	7.63 [a]	7.47 [a]	7.58 [a]	8.20 [a]	8.58 [a]	9.02 [a]	9.41 [a]	10.46	11.86
500	7.22 [a]	6.87 [a]	7.10 [a]	6.94 [a]	7.05 [a]	7.65 [a]	8.02 [a]	8.43 [a]	8.88 [a]	9.32	11.53
550	6.04 [a]	5.71 [a]	5.97 [a]	5.83 [a]	5.95 [a]	6.48 [a]	6.82 [a]	7.19 [a]	7.70 [a]	7.91 [a]	9.57
600	5.09 [a]	4.82 [a]	5.08 [a]	4.96 [a]	5.08 [a]	5.54 [a]	5.85 [a]	6.18 [a]	6.71 [a]	6.77 [a]	8.43 [a]
700	3.69 [a]	3.52 [a]	3.75 [a]	3.68 [a]	3.78 [a]	4.11 [a]	4.37 [a]	4.65 [a]	5.12 [a]	5.08 [a]	6.55 [a]
800	2.69 [a]	2.64 [a]	2.80 [a]	2.78 [a]	2.86 [a]	3.07 [a]	3.29 [a]	3.53 [a]	3.90 [a]	3.87 [a]	5.04 [a]
900	1.94	1.99	2.09	2.12 [a]	2.18	2.29 [a]	2.48 [a]	2.69 [a]	2.94 [a]	2.97 [a]	3.81 [a]
1000	1.48	1.54	1.60	1.62	1.68	1.71	1.88	2.03 [a]	2.16 [a]	2.27 [a]	2.78 [a]
1100	1.08	1.15	1.20	1.22	1.27	1.30	1.42	1.52	1.59	1.72	1.92
1200	0.73	0.79	0.84	0.86	0.90	0.95	1.03	1.09	1.16	1.27	1.41
1300	0.44	0.47	0.52	0.54	0.57	0.62	0.68	0.72	0.79	0.87	0.96

(c) $(1-x)Li_2O$–$(x)Na_2O$–$1.5SiO_2$ series [$\log(\eta_L/\text{Pa s})$]

x:	0.0	0.1	0.2	0.3	0.4	0.5	0.6	0.7	0.8	0.9	1.0
T(°C)											
600	5.39 [a]	4.83 [a]	4.83 [a]	4.34 [a]	4.22 [a]	4.52 [a]	4.49 [a]	4.70 [a]	4.79 [a]	5.26 [a]	5.81 [a]
700	3.71 [a]	3.37 [a]	3.41 [a]	3.03 [a]	2.97 [a]	3.20 [a]	3.22 [a]	3.40 [a]	3.50 [a]	3.84 [a]	4.24 [a]
800	2.57 [a]	2.37 [a]	2.42 [a]	2.13 [a]	2.11 [a]	2.28 [a]	2.32	2.47	2.57 [a]	2.81 [a]	3.13 [a]
900	1.76 [a]	1.64 [a]	1.68 [a]	1.47 [a]	1.47 [a]	1.59	1.64	1.77	1.86	2.03	2.29
1000	1.14 [a]	1.09 [a]	1.11 [a]	0.97	0.98	1.06	1.12	1.22	1.31	1.42	1.63
1100	0.66 [a]	0.65	0.66	0.58	0.60	0.65	0.70	0.78	0.86	0.93	1.11
1200	0.27	0.30	0.30	0.26	0.29	0.31	0.36	0.42	0.50	0.53	0.68
1300	−0.04	0.01	−0.01	0.01	0.03	0.03	0.08	0.12	0.19	0.19	0.32

Table 3 (continued)

(d) $(1-y)(0.4Li_2O \cdot 0.6Na_2O)$–$(y)K_2O$–$1.5SiO_2$ series [$\log(\eta_L/\text{Pa s})$]

y:	0.0	0.1	0.2	0.3	0.4	0.5	0.6	0.7	0.8	0.9	1.0
T(°C)											
600	4.49 [a]	4.35 [a]	4.32 [a]	4.46 [a]	4.45 [a]	4.67 [a]	4.91 [a]	5.30 [a]	5.68 [a]	6.31 [a]	7.59 [a]
700	3.22 [a]	3.18 [a]	3.18 [a]	3.30 [a]	3.29 [a]	3.42 [a]	3.66 [a]	3.96 [a]	4.23 [a]	4.74 [a]	5.62 [a]
800	2.32 [a]	2.34 [a]	2.35 [a]	2.44 [a]	2.44 [a]	2.52 [a]	2.75 [a]	2.97 [a]	3.16 [a]	3.57 [a]	4.19 [a]
900	1.64	1.70	1.72	1.79	1.79	1.83	2.05	2.21	2.34	2.67 [a]	3.09 [a]
1000	1.12	1.19	1.23	1.27	1.28	1.29	1.50	1.60	1.68	1.95	2.23
1100	0.70	0.79	0.83	0.85	0.86	0.85	1.05	1.11	1.15	1.37	1.54
1200	0.36	0.46	0.50	0.50	0.51	0.49	0.68	0.70	0.71	0.88	0.97
1300	0.08	0.18	0.22	0.21	0.22	0.19	0.37	0.36	0.34	0.47	0.49

[a] Interpolated values calculated from T_g and high-temperature viscosity values of the $(1-x)Li_2O$–$(x)Na_2O$–$2SiO_2$ series (a), $(1-y)(0.4Li_2O \cdot 0.6Na_2O)$–$(y)K_2O$–$2SiO_2$ series (b), $(1-x)Li_2O$–$(x)Na_2O$–$1.5SiO_2$ series (c) and $(1-y)(0.4Li_2O \cdot 0.6Na_2O)$–$(y)K_2O$–$1.5SiO_2$ series (d).

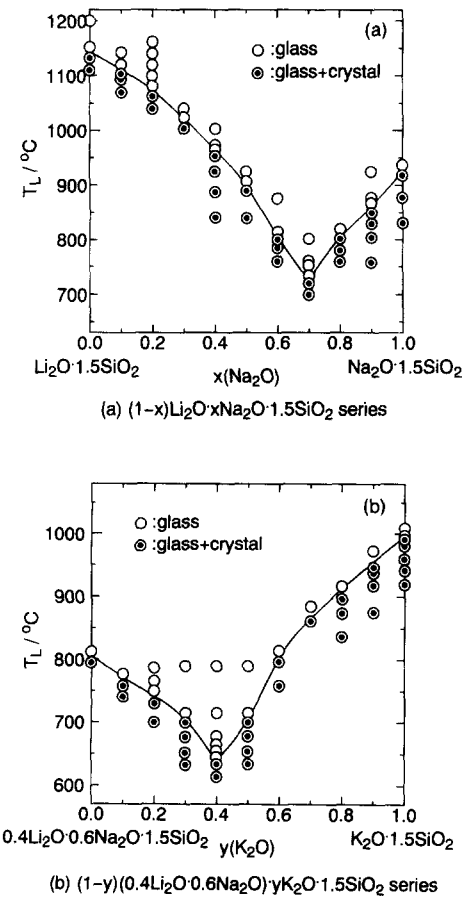

Fig. 4. Liquidus temperature (solid line) of the $(1-x)Li_2O$–$(x)Na_2O$–$1.5SiO_2$ series (a) and $(1-y)(0.4Li_2O \cdot 0.6Na_2O)$–$(y)K_2O$–$1.5SiO_2$ series (b). Open circles (○) denote glass and double circles (◎) partially crystallized glass.

and in a range of 600–1300°C in Table 3(c)–(d). Interpolated viscosity values at 440–1000°C were estimated by the Fulcher type viscosity equation $\log \eta_L = A + B/(T - T_0)$, using T_g and high-temperature viscosity data. Fig. 5(a) exhibits a shallow viscosity minimum at middle compositions around $x = 0.5$ in the 1000–1300°C range, and a deep minimum in the 420–600°C range. Fig. 5(b) shows that the isothermal viscosity increases progressively with increase of K_2O content in the 900–1300°C range, but a viscosity minimum appears in the 400–600°C range. Figs. 6(a) and (b) show that there is a viscosity minimum in the 600–900°C range, but the minimum disappears in the 1200–1300°C range.

The variations of T_g with composition in the Li_2O–Na_2O–K_2O–$mSiO_2$ systems ($m = 1.5$ or 2) are summarized in Table 2(a)–(d) and shown in Figs. 7(a) and (b). Fig. 7(a) shows that T_g becomes minimum at the composition $x = 0.7$–0.8 for $m = 2$, and the composition $x = 0.2$–0.3 for $m = 1.5$. Fig. 7(b) shows that T_g increases continuously with an increase of K_2O in the $(1-y)(0.4Li_2O \cdot 0.6Na_2O)$–$(y)K_2O$–$2SiO_2$ series, and becomes a minimum at the composition $y = 0.2$–0.4 composition in the $(1-y)(0.4Li_2O \cdot 0.6Na_2O)$–$(y)K_2O$–$1.5SiO_2$ series.

Liquidus viscosities, η_L, were obtained from T_L and the Fulcher type viscosity–temperature curve. η_L values are summarized in Table 2(a)–(d). The variation of η_L of the Li_2O–Na_2O–K_2O–$2SiO_2$ and the Li_2O–Na_2O–K_2O–$1.5SiO_2$ systems are shown in Figs. 8(a), (b) and 9(a), (b). Fig. 8(a) shows a η_L maximum, $\log(\eta_L/\text{Pa s}) = 3.2$ at the

eutectic composition $x = 0.6$. Fig. 8(b) shows a η_L maximum, $\log(\eta_L/\text{Pa s}) = 4.56$ at the eutectic composition $y = 0.5$. Fig. 9(a) shows a η_L maximum,

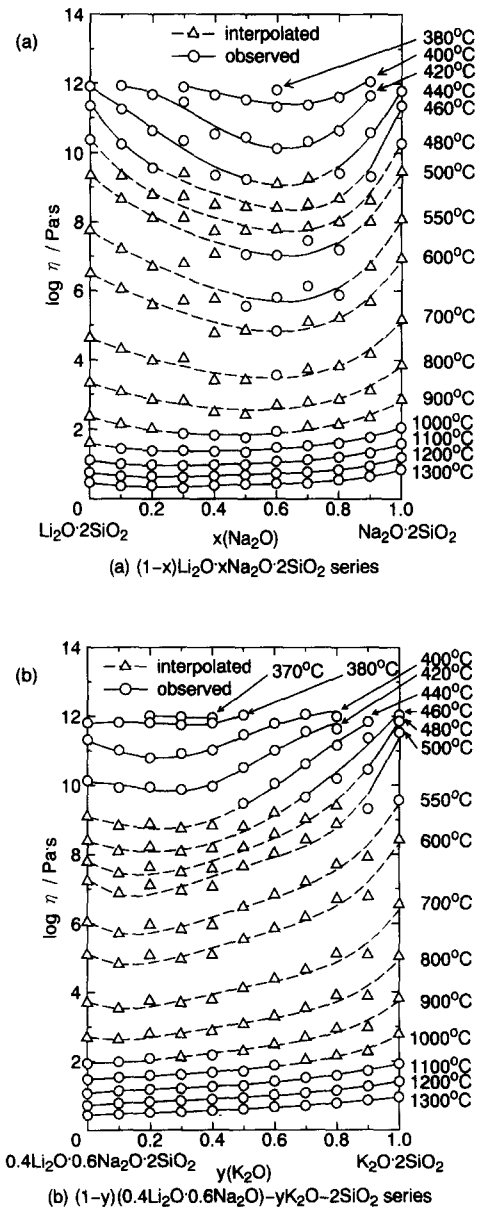

Fig. 5. Isothermal viscosities in the temperature range 370–1300°C of the $(1-x)Li_2O$–$(x)Na_2O$–$2SiO_2$ series (a) and $(1-x)(0.4Li_2O \cdot 0.6Na_2O)$–$(y)K_2O$–$2SiO_2$ series (b). Open circles (○) and solid line indicate the observed values, and triangles (△) and broken line interpolated values from T_g and high-temperature viscosity values.

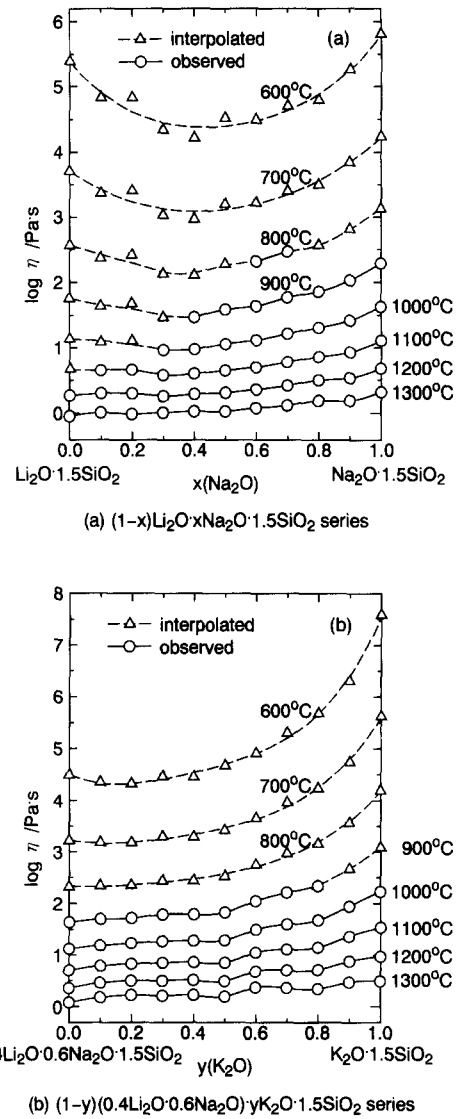

Fig. 6. Isothermal viscosities in the temperature range 600–1300°C of the $(1-x)Li_2O_{(x)}$–Na_2O–$1.5SiO_2$ series (a) and $(1-y)(0.4Li_2O \cdot 0.6Na_2O)$–$(y)K_2O$–$1.5SiO_2$ series (b). Open circles (○) and solid line indicate the observed values, and triangles (△) and broken line interpolated values from T_g and high-temperature viscosity values.

$\log(\eta_L/\text{Pa s}) = 3.2$, at the eutectic composition $x = 0.7$. Fig. 9(b) shows a η_L maximum, $\log(\eta_L/\text{Pa s}) = 4.0$, at the eutectic composition $y = 0.4$.

Log η_L values are plotted against log Q^* values in Fig. 10. A linear relationship is observed with a

slope of approximately d log η_L/d log $Q^* = -0.5$. This is consistent with the general relationship, that is, a greater liquidus viscosity corresponds to a smaller critical cooling rate and vice versa. The broken line indicates a slope -0.5, and the η_L–Q^* relationship is expressed as

$$\log \eta_L = -0.5 \log Q^* + 1.5 \pm 0.5.$$

4. Discussion

The fusion entropy, ΔS_f, consists of the configurational entropy, ΔS_{conf}, and the thermal entropy, ΔS_{th}. ΔS_{conf} includes the mixing entropy ΔS_m which arises from the mixed alkali ions. In the mixed alkali system, if the compositional dependence of ΔS_{conf} is affected by ΔS_m, the compositional dependence of ΔS_f is affected by ΔS_m. T_L is determined from the fusion enthalpy ΔH_f and ΔS_f when ΔH_f changes monotonically with composition, then a T_L minimum should result when ΔS_m assumes a maximum. ΔS_m can be calculated according to the regular solution model assuming certain glass constituents. Glass constituents may be deduced from the primarily precipitated compounds in the glass. By heat treatments (600°C, 650°C for 2–20 h) of the Li_2O–Na_2O–$2SiO_2$ glasses, $Li_2O \cdot 2SiO_2$ crystal along with $Li_2O \cdot SiO_2$ crystal precipitated in the Li_2O-rich compositions, and $Na_2O \cdot 2SiO_2$ crystal in the

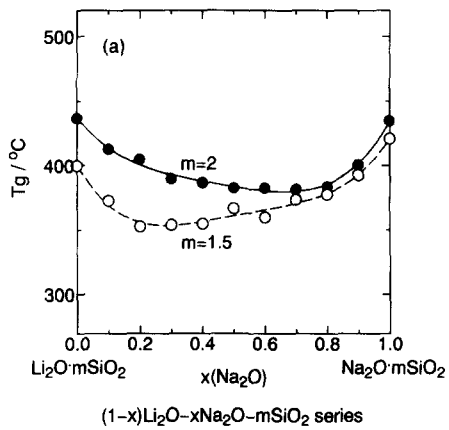

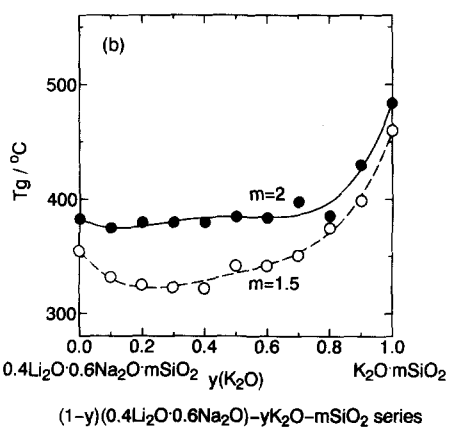

Fig. 7. Glass transition temperature, T_g, of the $(1-x)Li_2O$–$(x)Na_2O$–$mSiO_2$ series (a) and $(1-y)(0.4Li_2O \cdot 0.6Na_2O)$–$(y)K_2O$–$mSiO_2$ series (b). Closed circle (●) is for $m = 2$ and open circle (○) for $m = 1.5$.

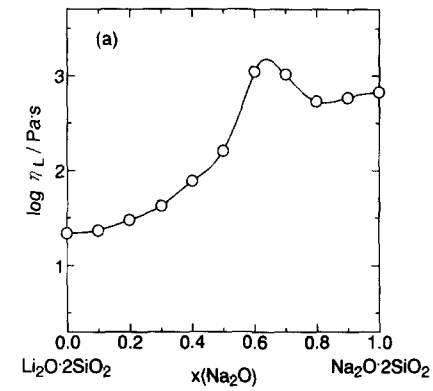

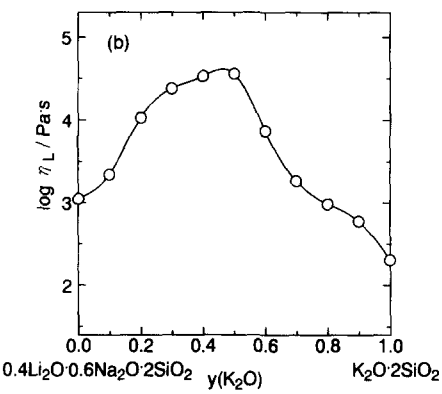

Fig. 8. Liquidus viscosity, η_L, of the $(1-x)Li_2O$–$(x)Na_2O$–$2SiO_2$ series (a) and $(1-y)(0.4Li_2O \cdot 0.6Na_2O)$–$(y)K_2O$–$2SiO_2$ series (b).

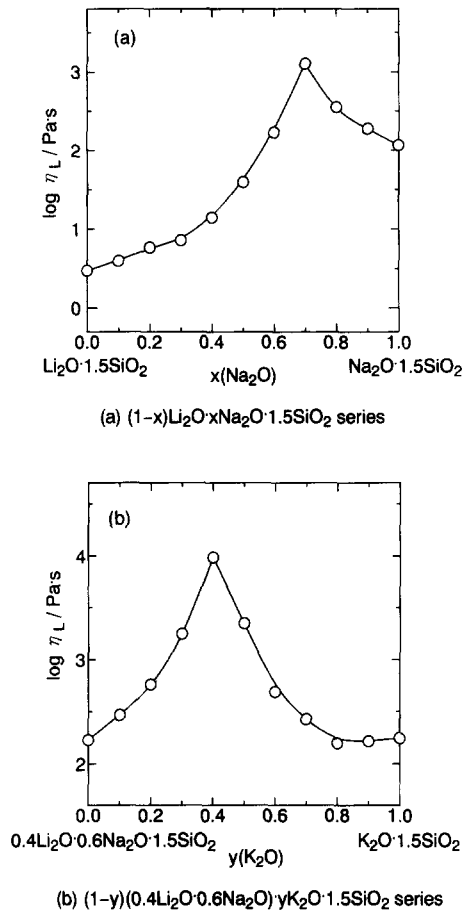

Fig. 9. Liquidus viscosity, η_L, of the $(1-x)Li_2O$–$(x)Na_2O$–$1.5SiO_2$ series (a) and $(1-y)(0.4Li_2O \cdot 0.6Na_2O)$–$(y)K_2O$–$1.5SiO_2$ series (b).

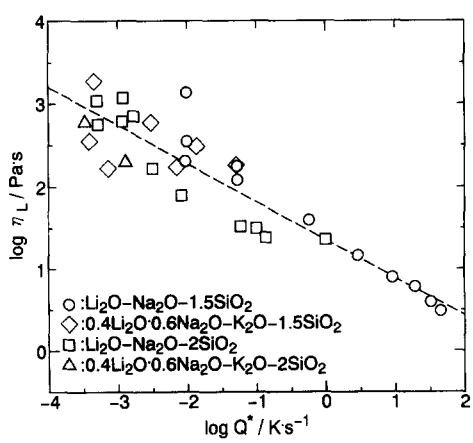

Fig. 10. Relationship between η_L and Q^* for glass formation in the Li_2O–Na_2O–K_2O–$mSiO_2$ system ($m = 2$ or 1.5).

Na_2O-rich compositions [18]. No phase change was observed in the primarily deposited phases during prolonged heating. On cooling the Li_2O–Na_2O–$1.5SiO_2$ melts, $Li_2O \cdot SiO_2$, and $Na_2O \cdot SiO_2$ crystals together with unknown crystals precipitated in the Li_2O-rich compositions, and $Na_2O \cdot SiO_2$ and $Na_2O \cdot 2SiO_2$ crystals together with a $Li_2O \cdot SiO_2$ crystal in the Na_2O-rich compositions. On the other hand, on cooling the $0.4Li_2O \cdot 0.6Na_2O$–K_2O–$1.5SiO_2$ melts, $Li_2O \cdot SiO_2$, $Na_2O \cdot SiO_2$ and $Na_2O \cdot 2SiO_2$ crystals precipitated in the compositions poor in K_2O, and a $K_2O \cdot 2SiO_2$ crystal and an unknown crystal in the compositions rich in K_2O. It is speculated from these crystals that glass constituents are $M_2O \cdot 2SiO_2$ and $M_2O \cdot SiO_2$ (M = Li, Na and K) components. However, the exact concentration of the $M_2O \cdot 2SiO_2$ and $M_2O \cdot SiO_2$ components cannot be estimated. To a first approximation, therefore, the glass constituents are assumed to be Li_2O–$mSiO_2$, Na_2O–$mSiO_2$ and K_2O–$mSiO_2$ units ($m = 1.5$ or 2) in the $(1-x)Li_2O$–$(x)Na_2O$–$mSiO_2$ and $(1-y)(0.4Li_2O \cdot 0.6Na_2O)$–$(y)K_2O$–$mSiO_2$ series. Then the mixing entropy, ΔS_m, among the Li_2O–$mSiO_2$ and Na_2O–$mSiO_2$ units may be given as

$$\Delta S_m = -R\{x \ln x + (1-x) \ln(1-x)\}, \quad (1)$$

where R is the gas constant and x is the molar fraction of the Na_2O–$mSiO_2$ unit ($m = 1.5$ or 2). Eq. (1) produces a maximum value $R \ln 2$ at the composition $x = 0.5$. If the compositional dependence of ΔS_m very strongly affects the compositional dependence of ΔS_f, the $(1-x)Li_2O$–$(x)Na_2O$–$mSiO_2$ series should show a eutectic at $x = 0.5$. In fact, a eutectic is observed at $x = 0.6$ ($m = 2$) and at $x = 0.7$ ($m = 1.5$), even though $x = 0.6$ is somewhat larger than the predicted composition $x = 0.5$ for $m = 2$. For the $(1-y)(0.4Li_2O \cdot 0.6Na_2O)$–$(y)K_2O$–$mSiO_2$ series, ΔS_m among the Li_2O–$mSiO_2$, Na_2O–$mSiO_2$ and K_2O–$mSiO_2$ units may be given as

$$\Delta S_m = -R\{0.4(1-y) \ln 0.4(1-y) + 0.6(1-y) \ln 0.6(1-y) + y \ln y\}, \quad (2)$$

where y is the molar fraction of the K_2O–$mSiO_2$ unit. Eq. (2) gives a maximum value of $1.09R$ at $y = 0.34$. In fact, a eutectic is observed at $y = 0.4$–0.5, which is somewhat larger than the predicted one, though the gaps between the theoretical and

observed eutectic compositions should be due to the oversimplification of the structural constituents assumed and the ambiguity of their concentrations.

5. Conclusion

The critical cooling rate corresponds to the liquidus viscosity in the mixed alkali silicate systems. It was found that mixed alkali silicate Li_2O–Na_2O–$m SiO_2$ shows a larger glass-forming ability than the single alkali silicate Li_2O–$m SiO_2$, Na_2O–$m SiO_2$ or K_2O–$m SiO_2$. The quasi-ternary mixed alkali Li_2O–Na_2O–K_2O–$m SiO_2$ shows an even larger glass-forming ability than Li_2O–Na_2O–$m SiO_2$. The significant role of ΔS_m or η_L in glass-forming kinetics was verified. Based on the present results we predict that the more numerous the components incorporated, the more easily will a glass result, provided that the components are mutually miscible.

Appendix

The theoretical background for the relationship between critical cooling rate and liquidus viscosity is introduced [6]. The crystal portion, $X(0)$, in the cooled sample must be smaller than the 10^{-4}–10^{-6} level when the melt is cooled at the critical cooling rate, Q^*. Q^* may be calculated by Eq. (3), where $X(0)$ assumes a value of the order of 10^{-4}–10^{-6}:

$$X(0) = 4\pi/3Q^{*4} \int I\left(\int U \, dT\right)^3 dT, \tag{3}$$

where I is the steady-state, homogeneous nucleation rate [6] and U is the crystal growth rate [6] given by Eqs. (4) and (5), respectively:

$$I = \left(32\alpha^2 n_0 RT\right)/\left(V\eta T_r^2 \, \Delta T_r^2\right) \times \exp\left(-16\alpha^3 \, \Delta S_f/3RT_r^3 \, \Delta T_r^2 - \Delta S_f/RT_r\right) \times \left\{1 - \exp\left(T_r \, \Delta T_r^2 \, \Delta S_f/2\alpha R\right)\right\} \tag{4}$$

$$U = \left(2RT/\eta N\pi a^2\right) \exp\left(-\Delta S_f/RT_r\right) \times \left\{1 - \exp\left(-T_r \, \Delta T_r^2 \, \Delta S_f/2\alpha R\right)\right\}, \tag{5}$$

where n_0 is the number of flow units per unit volume, N is Avogadro's number, R is the gas constant, ΔS_f is the fusion entropy per mole of flow units, η is the viscosity, V is the molar volume of flow units, a is the diameter of a flow unit, $T_r = T/T_L$ is the reduced temperature with respect to the liquidus temperature, T_L, and $\Delta T_r = 1 - T_r$ is the reduced undercooling. ΔS_f and V come into Eqs. (4) and (5) through an empirical relationship between the surface tension, σ, and the molar heat of fusion, ΔH_f, with a constant $\alpha = 0.3$–0.5 as given by Eq. (6):

$$\sigma = \Delta H_f/N^{1/3}V^{2/3}, = \alpha T_L \Delta S_f/N^{1/3}V^{2/3}. \tag{6}$$

Eqs. (4) and (5) are different from the existing equations [19–21] in several respects:

(a) the energy barrier, ΔG_c, for a flow unit to jump over the liquid–crystal boundary was assumed as $\Delta G_c = \Delta G_d + T_L \, \Delta S_f$, where ΔG_d is the activation energy for diffusion or viscous flow and $T_L \, \Delta S_f$ is the entropy barrier over the liquid–crystal interface. The probability for a flow unit to jump over the liquid–crystal interface is proportional to $\exp(-\Delta S_f/RT_r)$. The $\exp(-\Delta S_f/RT)$ term is included in Eqs. (4) and (5).

(b) ΔS_f is taken as a variable since the magnitude of ΔS_f is dependent on the size of the flow unit.

The temperature dependence of the viscosity was assumed to be Fulcher type, Eq. (7), with constants A, B and T_0:

$$\eta = A \exp(B/T - T_0) \tag{7}$$

Using the liquidus viscosity, η_L, activation energy for viscous flow, $E = R\,\mathrm{d}\ln\eta/\mathrm{d}(1/T)$ at T_L, Eq. (7) is described in the form:

$$\eta = \eta_L \exp E(1 - T_r)(1 - T_0/T_L)/RT_L(T_r - T_0/T_L). \tag{8}$$

Numerical calculation of Eq. (3) showed that Q^* can be expressed, to a first approximation, as a linear function of the liquid parameters η_L, E/T_L, T_0/T_L, ΔS_f, T_L and V for ΔS_f values greater than $0.5R$ as shown in Eq. (9):

$$\begin{aligned}\log Q^*(\mathrm{K/s}) = &-\log \eta_L(\mathrm{Pa\ s}) - 0.014E/T_L(\mathrm{J/K\ mol}) \\ &- 3T_0/T_L - 9.1\alpha^3 \, \Delta S_f(\mathrm{J/K\ mol}) \\ &+ 2\log T_L(\mathrm{K}) - \log V(\mathrm{m^3/mol}) \\ &- 0.25 \log X(0) - 2 \pm 0.5,\end{aligned} \tag{9}$$

where $X(0) = 10^{-4}$–10^{-6}.

References

[1] R. Ota and M. Kunugi, in: Proc. 11th Int. Conf. on Glasses, Prague (1977) p. 249.
[2] R. Ota and N. Soga, Yogyo-Kyokai-Shi 91 (1983) 265.
[3] R. Ota and N. Soga, Yogyo-Kyokai-Shi 89 (1981) 218.
[4] R. Ota and N. Soga, J. Soc. Mater. Sci., Jpn (Zairyo) 30 (1981) 600.
[5] R. Ota and N. Soga, Yogyo-Kyokai-Shi 90 (1982) 531.
[6] R. Ota, T. Kato and N. Soga, Yogyo-Kyokai-Shi 91 (1983) 73.
[7] R. Ota, H. Kozuka and N. Soga, Yogyo-Kyokai-Shi 92 (1984) 10.
[8] R. Ota, H. Tashiro and N. Soga, Yogyo-Kyokai-Shi 94 (1986) 249.
[9] R. Ota and N. Soga, J. Non-Cryst. Solids 95&96 (1987) 465.
[10] R. Ota and N. Soga, in: Proc. 14th Int. Conf. on Glasses, New Delhi, Vol. 1, (1986) p. 74.
[11] R. Ota, J. Murakami, S. Ichimura and J. Fukunaga, Molten Salts 34 (1991) 17.
[12] A.C. Havermans, H.N. Stein and J.H. Stevels, J. Non-Cryst. Solids 51 (1970) 66.
[13] O.V. Mazurin, Fiz. Stekla 6 (1980) 628.
[14] R. Ota and N. Soga, Glastechn. Ber. 56K (1983) 776.
[15] R. Ota, B. Tsuchiya, K. Kawamura, S. Nakanishi and J. Fukunaga, J. Ceram. Soc. Japan 99 (1991) 168.
[16] F.C. Kracek, J. Am. Chem. Soc. 61 (1939) 2874.
[17] A.R. West, J. Am. Ceram. Soc. 59 (1976) 124.
[18] R. Ota and J. Fukunaga, Advances in the Fusion of Glass, (American Ceramic Society, Westerville, OH, 1988) p. 31.1.
[19] D. Turnbull and M.H. Cohen, Modern Aspects of the Vitreous States, Vol. 1, ed. J.D. Mackenzie (Butterworth, London, 1960), p. 38.
[20] D. Turnbull and M.H. Cohen, J. Chem. Phys. 29 (1958) 1049.
[21] C.G. Bergewn, Introduction to Glass Science, ed. L.D. Pye, H.J. Stevens and W.C. LaSource (Plenum, New York, 1972) p. 173.